Interaction Between 3-T MRI Systems and Patients with an Implanted Pacemaker

S. Pisa and E. Piuzzi

Department of Information Engineering, Electronics and Telecommunications
Sapienza University of Rome, Rome, 00184, Italy
pisa@diet.uniroma1.it, piuzzi@diet.uniroma1.it

Abstract ─ In this paper, a transverse electro-magnetic (TEM) coil operating at 128 MHz in a 3-T magnetic resonance imaging system has been studied in terms of the interaction with patients with or without an implanted pacemaker. The pacemaker has been simulated as a copper box with a catheter constituted by an insulated copper wire with an uncapped tip and it has been placed inside either box or anatomical models of the thorax. Electromagnetic and thermal simulations have been performed by using finite difference time domain codes. The obtained results show that in the absence of the pacemaker, and for a radiated power producing in the box a whole body specific absorption rate (SAR) of 1 W/kg, that is a typical value for MRI examinations, the coil produces in the anatomical models peak temperature values lower than the limits issued by the International Electrotechnical Commission (IEC). In the presence of the pacemaker, temperature increments at the catheter tip in excess of those issued by the IEC standard are obtained when the MRI scanned area involves the pacemaker region. The 3-T coil produces lower SAR and temperature increments with respect to a 64-MHz (1.5-T system) birdcage antenna in patients with implanted pacemaker.

Index Terms ─ Cardiac pacemakers, dosimetry, magnetic resonance imaging (MRI), temperature.

I. INTRODUCTION

Magnetic resonance imaging (MRI) is the primary tool for the diagnosis of a wide number of diseases. However, MRI is contraindicated for patients implanted with pacemakers and implantable cardioverter defibrillators [1-3]. The most adverse effect seems to be the heating of the heart tissue around the catheter tip produced by the high currents induced on the catheter by the RF field used in the MRI technique [4-6].

The International Electrotechnical Commission (IEC) [7] considers that, to prevent tissue damage in the body, the radiofrequency field should induce temperature increases in the body core lower than 0.5 °C for normal operating mode and 1 °C for first level controlled operating mode, where medical supervision of the patient is required. Moreover, local tissue temperature should not exceed 39 °C and 40 °C for normal and first level controlled operating modes, respectively. Consequently, in [7] limitations have been reported with reference to the specific absorption rate (SAR). In particular, the whole body SAR (SAR_{WB}) should not exceed 2 W/kg and 4 W/kg in normal and first level controlled operating modes, respectively.

Most of MRI systems in use operate at 1.5 T (corresponding to a Larmor frequency of about 64 MHz). For typical RF sequences used in MRI the IEC limits are usually satisfied in terms of SAR and temperature [8-11]. However, if a subject with an implanted pacemaker is exposed to MRI radiofrequency (RF) fields, temperatures well above the IEC limits are reached at the catheter tip [12-17].

The last generation of MRI apparatus works with 3-T static magnetic field (Larmor frequency of about 128 MHz) [18-20]. To the Authors' knowledge, only few studies have been performed to investigate possible effects, on patients with metallic implants, due to 128 MHz MRI apparatus [21-23]. In [21], sixteen patients with pacemakers underwent 3-T MRI scanning of a region far from the one interested by the pacemaker, with a whole body system and with SAR limitation to 2 W/kg, without significant effects. In [22], a box phantom containing a vagus nerve stimulation catheter was exposed within a 3-T whole body coil with a 3 W/kg SAR. Temperature increments up to 14.7 °C were obtained after 15 minutes of exposure. Also in this case, the highest temperature increments were obtained when the scanned region was involving the catheter leads. Finally, a numerical study was performed in [23] to investigate possible effects due to 128 MHz apparatus on a realistic torso model obtaining temperature increments lower than 0.128 °C. In this case, vagus a very simplified pacemaker and coil model was used and no information on the radiated power was given.

In this paper, the interaction between the 128 MHz field of MRI apparatus and pacemakers will be studied

Submitted On: July 1, 2014
Accepted On: February 23, 2015

by using a numerical technique with realistic antenna, body and pacemaker models. Moreover, a comparison between SAR and temperature increments produced by 128 MHz and 64 MHz coils will be performed.

II. ELECTROMAGNETIC AND THERMAL MODELS

The radiofrequency antenna used in this work to generate the electromagnetic (EM) field needed for MRI examinations is a shielded transverse electromagnetic (TEM) coil [18,19]. The coil external diameter is 78 cm, and the height 80 cm (see Fig. 1 (a)). The TEM coil is constituted by 16 cylindrical copper legs with a diameter of 2 cm and a height of 65 cm (see Fig. 1 (b)). The legs are equidistant on a cylindrical surface with a diameter of 70 cm. The legs are connected, by tuning capacitances (C_T in Fig. 1 (c)), to two rings (with a 2 cm × 4 cm cross-section) that are in contact with the external shield. The capacitances are tuned to achieve the desired resonant frequency. Four 50 Ω generators (V_G in Fig. 1 (c)), sinusoidal in time, spaced apart by 90° and with 90° phase shift, are connected between the legs and the upper ring and are used for exciting the antenna at the frequency of 128 MHz. In correspondence of the generators, two tuning capacitances are used, one in series (C_S) and the other in parallel (C_P) to the generator ($C_T = C_S + C_P$) (see Fig. 1 (c)). This excitation simulates the one usually adopted in real coils [18,19], and produces a magnetic field with a circular clockwise polarization, with respect to the positive z-axis, necessary for maximum coupling with nuclear proton spin. A single generator with Gaussian time behavior is used for studying the frequency behavior of the reflection coefficient, from which the TEM resonance frequencies can be evaluated [18,19].

For sake of comparison, a 64 MHz low-pass birdcage coil has been also considered. The birdcage is identical to the TEM coil but the end rings are not in contact with the external shield. As a consequence, while in TEM coils the current paths close along the shield, in birdcages they close through the legs [24].

A box model (30×20×60 cm) and three 5-mm resolution anatomical models, derived from the Virtual Family (Duke) data set [25], have been considered.

The Duke anatomical model is a highly detailed and realistic model of the human body directly derived from MRI scans of a healthy volunteer. In particular, the three considered anatomical models are partial body models and are used for studying MRI exams targeting the thoracic, abdominal and head regions of the body. Figure 2 shows these models with their positioning inside the TEM coil without the shield. All the anatomical models have been obtained by positioning the Duke data set (110×58×360 cells and 78 different tissues) inside the TEM coil and removing body portions far from the coil where the RF power deposition is expected to be negligible. The use of the reduced models gives rise to consistent savings of memory occupation and execution times, in both EM and thermal simulations, without reducing the accuracy of the computed results [17].

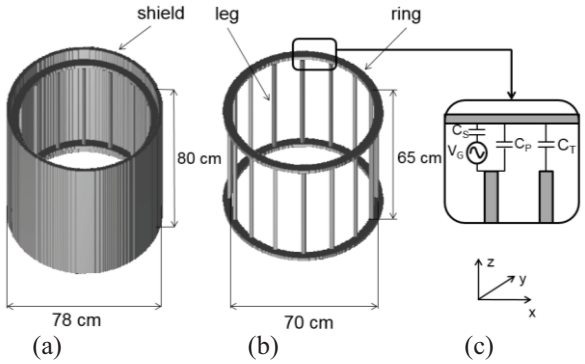

Fig. 1. (a) Shielded TEM coil, (b) TEM coil without the shield, and (c) zoom on the leg-ring connection region.

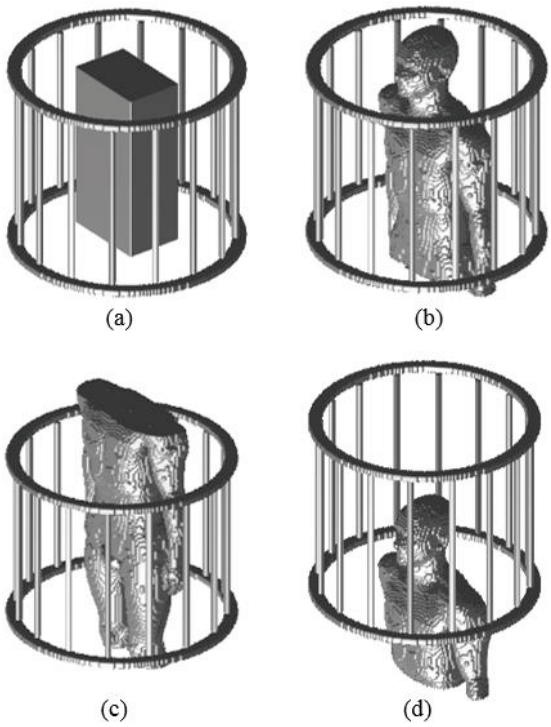

Fig. 2. (a) Box model, and three anatomical models corresponding to MRI exams targeting the: (b) thoracic, (c) abdominal, and (d) head regions of the body with their positioning inside the TEM antenna with removed shield.

The considered pacemaker is constituted by a copper box (4×1×5 cm) equipped with a catheter (see

Fig. 3 (a)). The catheter consists of a cylindrical copper wire with a diameter of 0.8 mm. The copper wire is covered by an insulating material with an external diameter of 2 mm from which the last 2 mm before the catheter tip have been removed (uncapped catheter – UC). The UC geometry represents a good model of commercially available monopolar catheters [17].

In the human box model, the copper box is placed 1 cm below the box surface and the catheter is placed on the same plane as in a typical experimental set-up (see Fig. 3 (b)) [26].

In the anatomical models the pacemaker is inserted in the subcutaneous fat layers in the left part of the thorax with a placement, based on computed tomography (CT) scans of patients with pacemaker, approximating the clinical one (see Fig. 4) [27]. In the body placement, the catheter roughly follows the vein path to the heart cavities of the anatomical model and is inserted a few millimeters in the right ventricle internal wall. In order to avoid unrealistic crossing of the catheter through different tissues, the vein path has been slightly modified at some points by adding cylindrical blood vessels of 3 mm diameter. This ensures that the catheter is always inserted into the vessels.

Electromagnetic simulations have been performed using a code based on a conformal FDTD scheme with graded-mesh [28]. The FDTD domain has been closed applying a 4-layer uniaxial perfectly matched layer (UPML) boundary condition with parabolic profile and 1% nominal reflection coefficient [29]. The investigated region has been divided in cells of variable side, from 0.5 mm (around the catheter) to 5 mm. For the permittivity, conductivity, and density data of the 78 Duke tissues, the values in [30] have been considered. At 128 MHz the wavelength in the tissue with the highest permittivity is about 28 cm. Hence, the maximum cell size (5 mm) corresponds to about 1/50 of the wavelength, resulting in a phase-spread ratio better than 0.999 for all propagation angles.

In all the simulations performed for the evaluation of the SAR distributions, a 128 MHz harmonic excitation has been applied. Once steady state conditions are reached, the amplitude of the three electric field components is determined, in the center of each cell, and the SAR distribution is calculated [17]. The evaluated SAR values are the peak SAR averaged over the mass of 1 FDTD cell (0.125 g - $SAR_{0.125g}$ or 0.125 mg - $SAR_{0.125mg}$ depending on the used mesh), the peak SAR averaged over 10 g (SAR_{10g}), and the SAR averaged over the whole body (SAR_{WB}), which is the quantity to be evaluated for assessing the compliance with IEC standard [7].

The temperature distribution T = T(r,t), inside the considered body models, has been computed by using the bioheat equation (BHE) [31,32]. To obtain a finite-difference formulation of the BHE, the body model is divided in cells of variable side, equal to those used in the FDTD computations, and the temperature is evaluated in a grid of points defined at the center of the cells. The BHE has been solved by using an alternate direction implicit finite difference (ADI-FD) formulation [17,33].

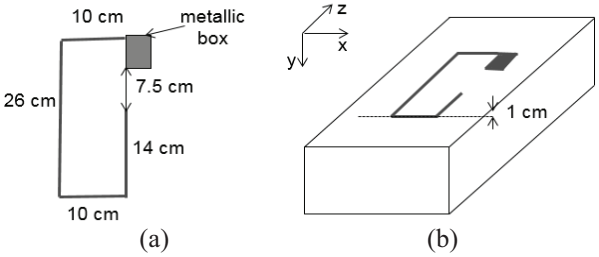

Fig. 3. (a) Pacemaker model, and (b) pacemaker positioning inside the box.

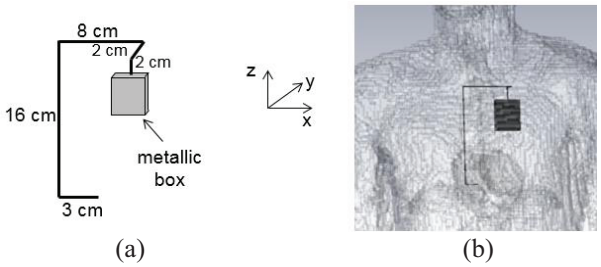

Fig. 4. (a) Pacemaker model, and (b) pacemaker positioning inside the thorax.

The numerical codes used in this paper for the solution of the EM and thermal problems in patients exposed to the field emitted by MRI antennas have been previously validated [16]. In particular, in [16] the SAR_{WB} values, computed by using the FDTD code in a box model of the human body exposed to a birdcage antenna, showed a very good agreement with measurements performed by means of a calorimetric set-up. Similarly, temperature time behaviors at the tip of a pacemaker placed inside a box model of the thorax, measured with a fluoroptic thermometer (Luxtron 3100), were in good agreement with thermal simulations performed with the ADI-FD code.

III. RESULS AND DISCUSSION

In all the simulations, the TEM coil has been tuned so that the mode with highest field homogeneity occurs at 128 MHz. This is accomplished by setting C_T = 9.34 pF, C_S = 4.67 pF, and C_P = 4.67 pF.

A. Box model without the pacemaker

The first considered thorax model is a parallelepiped box (30 cm × 20 cm × 60 cm) whose

electrical properties mimic those of an average human tissue at the considered frequency. Permittivity (ε), conductivity values (σ) and density (ρ) of the model are equal to 69.0, 0.62 S/m and 1006 kg/m^3, respectively. SAR values have been obtained for an antenna radiated power producing a SAR_{WB} of 1 W/kg (P_{RAD} = 40.8 W) that is a typical value for MRI examinations [10,16]. For the considered coil, the induced $SAR_{0.125g}$, and SAR_{10g} are 4.3, and 3.4 W/kg, respectively. Figure 5 (a) shows the SAR distribution on a coronal section passing 1 cm below the box surface (where the pacemaker will be placed). While Fig. 5 (b) shows the SAR distribution on the central axial section. Figure 5 (b) outlines that the highest local SAR values are achieved close to the external surface of the box and, in particular, for a circular left polarized EM field, they are close to the bottom-right and upper-left corners. It is worth noting that the SAR distribution does not show horizontal symmetry. In fact, while the structure is symmetric, the field excitation presents an azimuthal phase shift.

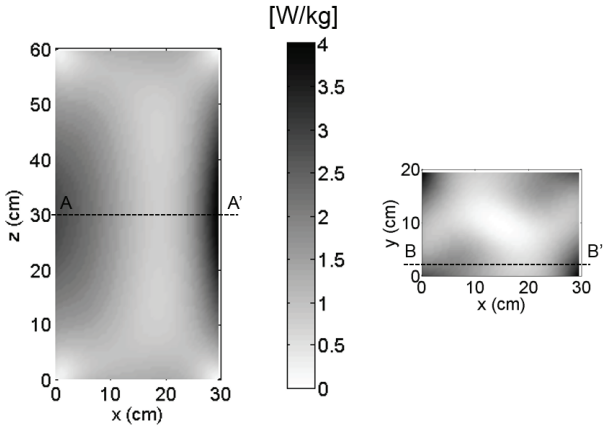

Fig. 5. (a) SAR distributions for the TEM coil on a coronal section 1 cm below the box surface, and (b) on the central axial section. (a) Corresponds to section B-B' in (b), and (b) corresponds to section A-A' in (a).

Thermal simulations have been performed by using the ADI-FD code with a box thermal conductivity (K) equal to 0.2 W/(m·°C), specific heat capacity (C) of 4178 J/(kg·°C) and neglecting the blood perfusion (B = 0). A convection coefficient equal to 10 W/(m^2·°C) has been also assumed at the air-box interface. Figure 6 shows the temperature distribution over the same coronal section of Fig. 5 (a). A maximum temperature increase of about 2.3 °C after 60 minutes of exposure has been observed. It is interesting to note that the highest temperature increments are achieved at the point where the peak SAR_{10g} is located (x = 28 cm, z = 30 cm). This is due to the fact that the point of the peak $SAR_{0.125g}$ (x = 30 cm, z = 30 cm) is close to the air-tissue interface where the thermal convection reduces the temperature increments.

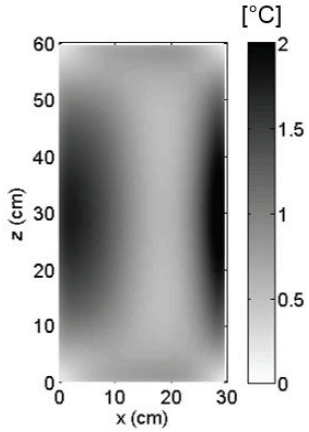

Fig. 6. Temperature distribution on a coronal section 1 cm below the box surface.

B. Anatomical models without the pacemaker

The first considered anatomical model is the one suitable for simulating an MRI examination at the level of the thorax (see Fig. 2 (b)). For a radiated power of 40.8 W (equal to that used for the box model of the thorax) about 35.5 W are absorbed in the reduced Duke.

Since the absorption in the remaining part of the body can be considered negligible, a SAR_{WB} of 0.49 W/kg can be extrapolated.

Figure 7 (a) shows the computed SAR distribution in a central coronal section. The peak $SAR_{0.125g}$ is 10.7 W/kg and has been obtained in the skin in the neck-shoulder region while the peak SAR_{10g} is 4.7 W/kg and has been obtained in the neck muscle.

Then, the second position (abdominal region examination) has been considered (see Fig. 2 (c)). The obtained results in terms of SAR are: 0.46, 6.2, 28.3 W/kg for the SAR_{WB}, SAR_{10g} and $SAR_{0.125g}$, respectively. Figure 7 (b) shows the SAR map in the central coronal section for this exposure. In this case, the peak $SAR_{0.125g}$ is located in the skin of the inguinal region and the peak SAR_{10g} in the leg muscle.

Finally, considering the head region examination (see Fig. 2 (d)), the obtained SAR_{WB}, SAR_{10g} and $SAR_{0.125g}$ have been 0.35, 8.2 and 26.2 W/kg, respectively. Figure 7 (c) shows the SAR map in the central coronal section. Similarly to the thorax examination, the peak $SAR_{0.125g}$ is located in the skin of the neck-shoulder region and the peak SAR_{10g} in the neck muscle.

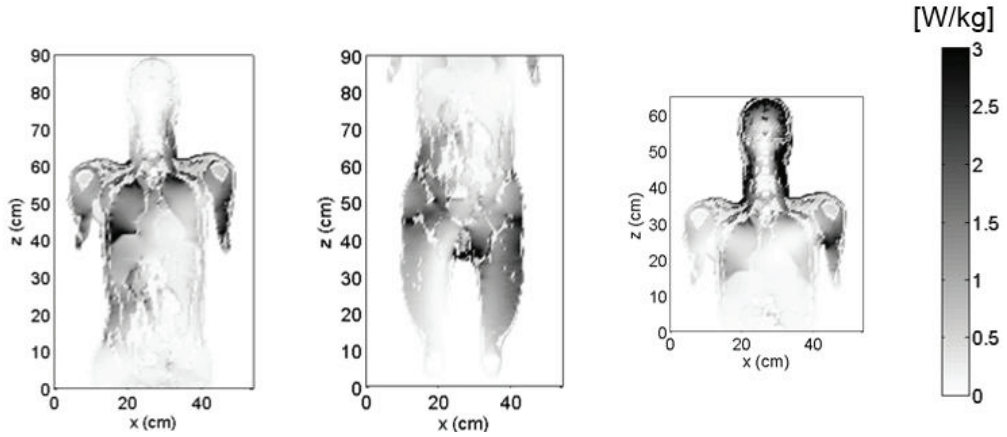

Fig. 7. SAR distributions on a central coronal section for the three models corresponding to MRI exams targeting the: (a) thoracic, (b) abdominal, and (c) head regions.

Starting from the obtained SAR results, temperature distributions have been computed in the absence and in the presence of perfusion by using the tissue thermal parameters available from [34]. The time behavior of temperature increment during a 1 hour MRI investigation has been computed at the points where the peak SAR are located. The considered exposure times are longer than those of a typical MRI examination, but have been considered in order to better evaluate the heating time constants. With reference to the thorax examination, Fig. 8 shows temperature increments as a function of time. The figure shows the strong limiting effect on temperature elevation of the blood perfusion. In fact the maximum temperature increment is 2.8 °C in the absence of perfusion and reduces to 1.1 °C when the blood perfusion is taken into account. The ratio between the maximum temperature increment in the absence and in the presence of perfusion is 2.5, very similar to that found in [35] by comparing measured temperature increases in a phantom model and in the human forearm. Moreover, both in the absence and in the presence of blood perfusion the highest temperature increments are obtained around the point where the SAR_{10g} is located.

Concerning the other two body positions, in the presence of blood perfusion, the T_{MAX} after one hour exposure is 1.1 °C and 1.8 °C for the abdomen and head examinations, respectively. It is important to note that the IEC SAR_{WB} limits for the normal and first level controlled operating modes are 2 W/kg and 4 W/kg, respectively. Due to the linearity of BHE, if these values are reached, temperature increments about 4 times and 8 times higher, with respect to those above reported, will be obtained. Under these conditions local tissue temperature limits issued by IEC for normal and first level controlled operating modes are overcome.

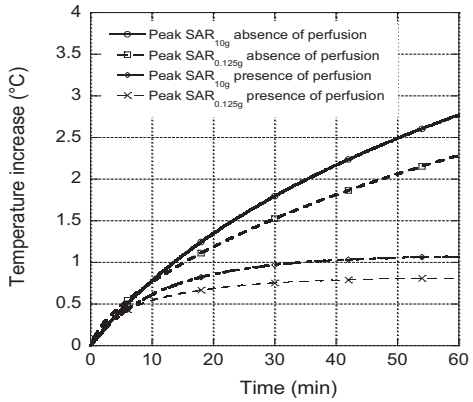

Fig. 8. Temperature time behaviour in the absence and in the presence of blood perfusion for the thorax examination.

C. Box model with the pacemaker

To study the exposure of a patient with an implanted pacemaker to a 3-T system, a pacemaker equipped with a unipolar catheter has been inserted inside the box model of the thorax in a typical operating position with the catheter tip 7.5 cm far from the pacemaker (see Fig. 3). The exposure has been studied exciting the coil with a power of 40.8 W that is the one producing a SAR_{WB} of 1 W/kg in the box in the absence of the pacemaker.

The current flowing along the catheter has been computed as the circulation of the magnetic field around the catheter axis. Figure 9 (a) shows the obtained current distribution. The distance along the wire from the point in which the catheter is inserted in the pacemaker is reported on the horizontal axis (the catheter length is 60 cm). The obtained current distribution can be explained observing that the current

inside the catheter wire is mainly produced by the electric field component, found in the absence of the wire (unperturbed field), parallel to the wire axis [13-17]. Moreover, for the considered 128 MHz field, the wavelength in the box tissue is about 28 cm, and hence, about half of the total wire length; this results in resonance phenomena along the wire. Finally, the maximum on the current behavior along the catheter, at distance equal to zero, can be explained as a short circuit effect of the pacemaker box, and the minimum at the catheter tip as an open end effect.

Figure 9 (b) shows the SAR distributions in a coronal section passing through the catheter. The figure outlines that the highest SAR values are obtained at the catheter tip. SAR_{WB}, peak $SAR_{0.125mg}$, and SAR_{10g} are 1.0, 7800, and 16.6 W/kg, respectively. In the presence of the pacemaker, the SAR_{WB} remains equal to the value without the pacemaker. To complete the dosimetry investigation, a thermal study has been then performed. In these simulations the tissue parameters used in the absence of the pacemaker have been employed. For the plastic insulation (p) and wire (w), instead, the values in [16] have been considered [$Cp = 1500$ J/(kg°C), $K_p = 0.2$ W/(m°C), $\rho_p = 1000$ kg/m^3; $C_w = 385$ J/(kg°C), $K_w = 401$ W/(m°C), $\rho_w = 8960$ kg/m^3]. The previously computed SAR distribution has been assumed as thermal source and a thermal transient analysis has been launched in the ADI-FD thermal solver for a duration of 15 minutes, that is the typical duration of an MRI examination [22].

Figure 10 (a) shows the time behavior of the simulated temperature along the catheter axis. After 15 minutes of exposure, a temperature increment of about 50 °C at a point just above the catheter tip has been obtained. The figure also outlines the reduction in temperature increase at points far from the tip.

Figure 10 (b) shows a map of the temperature distribution, after 15 minutes of exposure, on a coronal section passing through the pacemaker plane. The figure outlines a high temperature hot spot at the catheter tip and some lower hot spots in correspondence of the catheter bends.

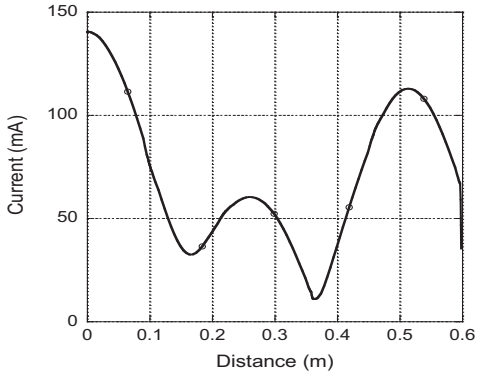

(a)

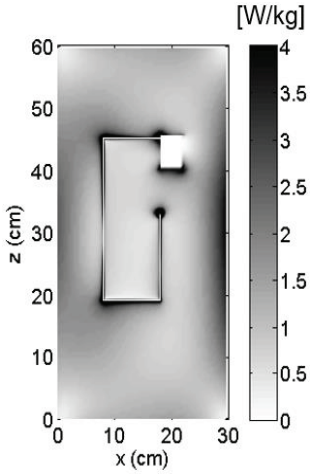

(b)

Fig. 9. (a) Current distribution along the catheter, and (b) SAR distribution on a coronal section 1 cm below the box surface.

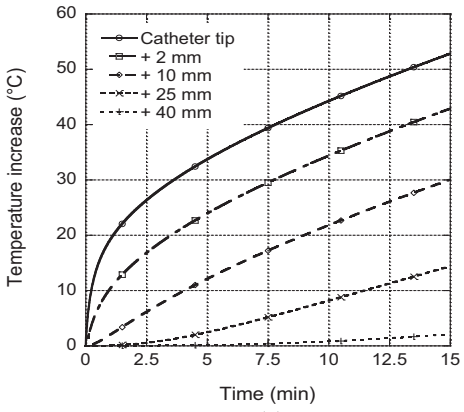

(a)

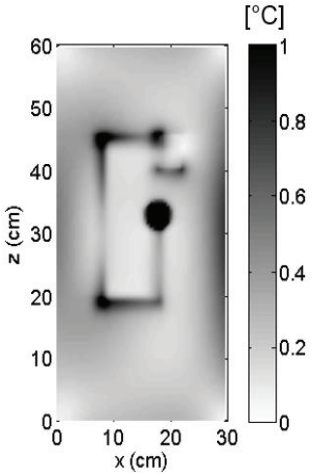

(b)

Fig. 10. (a) Temperature time behavior along the catheter axis, and (b) temperature distribution on a coronal section 1 cm below the box surface.

D. Anatomical models with the pacemaker

In order to achieve realistic SAR and temperature evaluations for a patient with an implanted pacemaker exposed to MRI fields, the pacemaker has been inserted inside the left part of the thorax of the Duke model, that in turn has been inserted inside the TEM coil and exposed to a 128 MHz left polarized field with a radiated power of 40.8 W (as for the box model). In particular, two configurations have been considered. In the first case (connected), the PM case is connected to the catheter as in Fig. 4 (a), while in the second case (disconnected), the first 2 cm of the catheter have been removed simulating the condition of a patient with the pulse generator not attached [36].

Figure 11 shows the current along the catheter, as a function of the distance from the point in which the catheter is inserted in the metallic box. In the considered cases the catheter length (31 cm) is comparable with the field wavelength in the body and only one resonance is present in the spatial current distribution. Moreover, a strong reduction in the current is observed in correspondence of the tip where the catheter is uncapped. The main difference between the two considered cases is the higher current along the catheter (78 mA versus 64 mA peak values) and at the catheter tip (20.9 mA versus 17.8 mA) of the disconnected case with respect to the connected one. Moreover, the short circuit effect of the PM case and the open end effect of the catheter tip, already evidenced in the previous section, are confirmed.

The computed $SAR_{0.125mg}$ at the catheter tip are 2670 W/kg and 3680 W/kg, while the SAR_{10g} are 5.5 W/kg and 7.5 W/kg for the connected and disconnected cases, respectively. These results confirm those in [36] where it was evidenced that the heating produced by MRI in patients with the pacemaker pulse generator disconnected was higher than that achieved when the pulse generator was attached. Similarly to the box exposure, the presence of the pacemaker does not affect significantly the SAR_{WB}. Moreover, the SAR distribution is similar to that in the absence of the pacemaker except for a strong hot spot at the catheter tip resulting from the high current densities induced in tissues around the tip.

Concerning the exposure of a patient with pacemaker when performing an examination at the level of the abdomen, a peak $SAR_{0.125mg}$ at the catheter tip of 510 W/kg has been computed. The peak SAR_{10g} is 6.2 W/kg, as in the absence of the pacemaker, while the SAR_{10g} at the catheter tip in the heart is 1.0 W/kg. Eventually, the SAR_{WB} is still 0.46 W/kg.

The exposure of a patient with pacemaker when performing an examination at the level of the head gives rise to SAR_{WB} and SAR_{10g} of 0.35 and 11.6 W/kg, as in the exposure without the pacemaker. The $SAR_{0.125mg}$ and SAR_{10g} at the catheter tip are 990 and 2.0 W/kg, respectively.

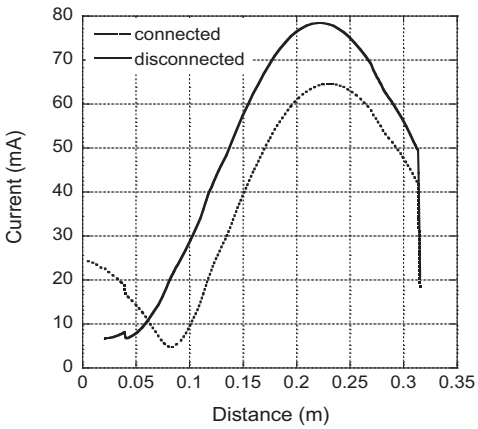

Fig. 11. Current distribution along the catheter inserted inside the left part of the thorax of the Duke model.

In order to assess the thermal risk associated with the computed SAR values, the graded mesh ADI solution of the bioheat equation has been applied. In this case, the heart-blood convection coefficient (HB) has been assumed equal to 1000 W/(m^2·°C) [37].

Figure 12 shows temperature versus time at the catheter tip, for the connected case, computed by neglecting the perfusion and in the presence of perfusion. In the first case, temperature increments of about 12 °C after 15 minutes exposure are obtained and the time behavior indicates an exponentially growing trend with a time constant of the order of hours. The presence of blood perfusion reduces temperature increments to about 3.0 °C and, in this case, the steady state is reached in a few minutes. In both considered cases, the temperature increments are higher than those indicated as safe in the IEC Standard [7].

Concerning the other two body positions, in the presence of blood perfusion, the T_{MAX} at the catheter tip after one hour exposure are 0.75 °C and 1.8 °C in the abdomen and head examinations, respectively.

These results indicate that only if the pacemaker is far from the coil center (as in the abdomen and head examinations) temperature increments, produced by the interaction of the RF field with the pacemaker, are compliant with the IEC limits. This result is in agreement with experimental findings [21,22] suggesting the possibility, for patients bearing a pacemaker, to perform MRI examinations when the region to scan is far from the pacemaker.

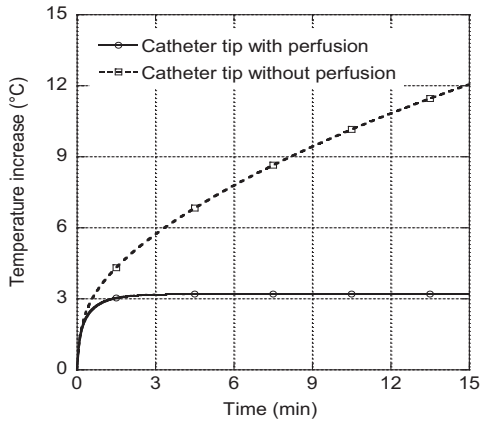

Fig. 12. Temperature time behavior at the catheter tip.

E. Comparison between TEM and birdcage coils

In order to compare the 3-T system with 1.5-T ones, some of the previously reported simulations have been repeated by using the 64 MHz birdcage coil previously described (see Section II).

In these simulations, the birdcage has been tuned to 64 MHz by using capacitances of 11.4 pF. Concerning the box simulations, permittivity and conductivity values of 78.2 and 0.6 S/m have been considered, respectively, while for the simulations with the Duke model the tissue permittivity and conductivity values in [30] have been used.

The results for the 128 MHz coil are reported in Table 1, 3rd column, while those for the 64 MHz coil in Table 1, 4th column. The table shows that in the absence of the pacemaker, SAR and temperature increments obtained at 128 MHz are slightly higher than those achieved at 64 MHz.

It is worth noting that, the reported SAR values have been obtained for an antenna-radiated power producing a SAR_{WB} of 1 W/kg in the box model. This radiated power gives rise in the box central region to magnetic fields of about 1.2 A/m and 1.6 A/m at 128 MHz and 64 MHz, respectively. TEM and birdcage coils can be compared considering the same RF magnetic field in the investigated sample. To this end, a value of 2.4 A/m has been chosen. This value is close to the typical mean field value necessary in MRI to produce a 90° flip angle in the sample [10]. Under these conditions, SAR_{WB} of 4 W/kg and 2.25 W/kg are obtained at 128 MHz and 64 MHz, respectively, with a SAR_{WB} ratio of 1.78, very similar to that found in [38] for a doubling of the frequency.

The presence of the pacemaker gives rise to higher SAR_{10g} and T_{MAX} in the birdcage coil with respect to the TEM one. This result can be explained comparing the SAR distributions of the box and of the anatomical model at 64 MHz reported in Fig. 13 (a) and (b) with the corresponding distributions at 128 MHz (see Fig. 5 (a) and 7 (a)). From the figures, the higher penetration depth of the 64 MHz field with respect to the 128 MHz one is evident. This, in turn, gives rise to higher currents at the catheter tip of the pacemaker exposed in the birdcage with respect to the TEM coil (22.4 mA versus 17.8 mA) and consequently to the higher SAR_{10g} and T_{MAX} at 64 MHz with respect to 128 MHz.

The superficial absorption of the 128 MHz field is also the responsible for the higher SAR and temperature increments in the TEM coil in the absence of the pacemaker.

Table 1: Comparison between TEM coils operating at 128 MHz and birdcage coils operating at 64 MHz

		3 T (128 MHz) TEM coil	1.5 T (64 MHz) Birdcage Coil
BOX	SAR_{WB}	1.0 W/kg	1.0 W/kg
//	SAR_{10g}	3.4 W/kg	2.9 W/kg
//	T_{MAX}	0.7 °C	0.6 °C
DUKE THOR.	SAR_{WB}	0.49 W/kg	0.46 W/kg
//	SAR_{10g}	4.7 W/kg	4.4 W/kg
//	T_{MAX} (WP)	1.1 °C	0.9
BOX + PM	SAR_{WB}	1.0 W/kg	1.0 W/kg
//	SAR_{10g}	16.6 W/kg	17.1 W/kg
//	T_{MAX}	53 °C	55 °C
D. THOR + PM	SAR_{WB}	0.49 W/kg	0.46 W/kg
//	SAR_{10g}	5.5 W/kg	14.0 W/kg
//	T_{MAX} (WP)	3 °C	8.3 °C

WP = with perfusion. T_{MAX} are temperatures after 15 min exposure.

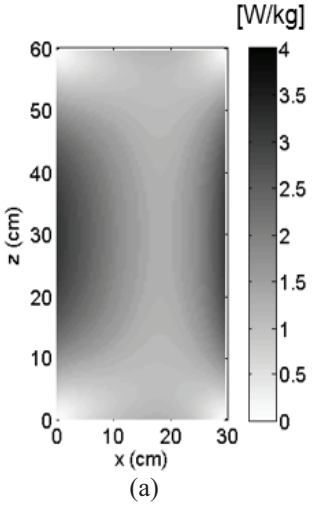

(a)

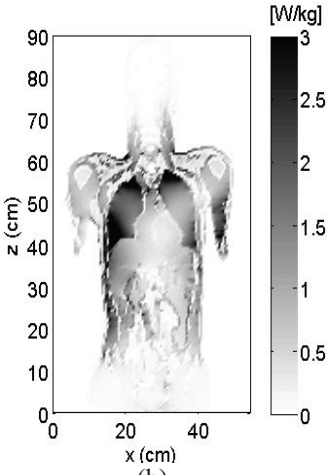

(b)

Fig. 13. (a) SAR distribution for the birdcage coil on a coronal section 1 cm below the box surface, and (b) on a central coronal section of the anatomical model (thoracic examination).

IV. CONCLUSION

In this paper, a TEM coil operating at 128 MHz in a 3-T MRI system has been studied in terms of the interaction with patients. A box model and an anatomical body model in different positions have been considered with or without the presence of an implanted monopolar pacemaker.

In the absence of the pacemaker, the power absorption in the box model is mainly concentrated in the external part of the box, while the region with highest temperature increments shows a slight shift towards the inner part of the box. The maximum temperature elevations in the box model are very similar to those obtained in the thorax model in the absence of blood perfusion. The highest SAR_{WB} have been obtained for the thorax examination and the lowest for the head one, while the opposite holds for the peak SAR_{10g} values.

The peak temperature increments computed inside the body in the presence of blood perfusion comply with IEC limits. However, if SAR_{WB} values are increased to the corresponding IEC limits for the normal and first level controlled operating modes, temperature limits would be overcome. Concerning the relation between maximum temperature increases and SAR_{10g}, the obtained results indicate a factor of about 0.2° C/(W/kg).

The insertion of a pacemaker inside the box model gives rise to very high peak $SAR_{0.125mg}$ and temperature increments in the absence of perfusion. The inclusion of the blood perfusion strongly reduces temperatures increments that, however, remain higher than IEC limits whenever the pacemaker is close to the coil center. In the presence of the pacemaker, high SAR values are achieved close to the catheter tip inside the heart. In this case, the factor linking the SAR_{10g} at the catheter tip to temperature increments is between 0.6 and 0.9 °C/(W/kg) depending on the SAR distribution.

A comparison between TEM coil and birdcage indicates that the 3-T TEM coil produces lower SAR and temperature increments with respect to a classic 64-MHz (1.5-T system) birdcage antenna for patients with implanted pacemaker.

REFERENCES

[1] ICNIRP Statement on: "Medical magnetic resonance (MR) procedures: protection of patients," *Health Phys*., vol. 87, pp. 197-216, 2004.

[2] J. R. Gimbel and E. Kanal, "Can patients with implantable pacemakers safely undergo magnetic resonance imaging?," *J. Am. Coll. Cardiol*., vol. 43, pp. 1325-1327, 2004.

[3] M. H. Schoenfeld, "Contemporary pacemaker and defibrillator device therapy: challenges confronting the general cardiologist," *Circulation*, vol. 115, pp. 638-653, 2007.

[4] S. Achenbach, B. Moshage, W. Diem, T. Bieberle, V. Schibgilla, and K. Bachmann "Effects of magnetic resonance imaging on cardiac pacemakers and electrodes," *Am. Heart. J*., vol. 134, pp. 467-473, 1997.

[5] T. Sommer, C. Vahlhaus, G. Lauck, A. von Smekal, M. Reinke, U. Hofer, W. Bloch, F. Traber, C. Schneider, J. Gieseke, W. Jung, and H. Schild, "MR imaging and cardiac pacemaker: in-vitro evaluation and in-vivo studies in 51 patients at 0.5 T," *Radiology*, vol. 215, pp. 869-879, 2000.

[6] A. Roguin, M. M. Zviman, G. R. Meininger, E. R. Rodrigues, T. M. Dickfeld, D. A. Bluemke, A. Lardo, R. D. Berger, H. Calkins, and H. R. Halperin, "Modern pacemaker and implantable cardioverter/defibrillator systems can be magnetic resonance imaging safe, in vitro and in vivo assessment of safety and function at 1.5 T," *Circulation*, vol. 110, pp. 475-482, 2004.

[7] International Electrotechnical Commission, International Standard, Medical Electrical Equipment–IEC 60601-2-33, *Particular Requirements for the Basic Safety and Essential Performance of Magnetic Resonance Equipment for Medical Diagnosis*, 3rd edition, Geneva: IEC, 2010.

[8] U. D. Nguyen, S. Brown, I. A. Chang, J. K. Krycia, and M. S. Mirotznik, "Numerical evaluation of heating of the human head due to magnetic resonance imaging," *IEEE Trans. Biomed. Eng*., vol. 51, pp. 1301-1309, 2004.

[9] W. Liu, C. M. Collins, and M. B. Smith, "Calculations of B1 distribution, specific energy

absorption rate, and intrinsic signal-to-noise ratio for a body-size birdcage coil loaded with different human subjects at 64 and 128 MHz," *Appl. Magn. Reson*., vol. 29, pp. 5-18, 2005.

[10] C. M. Collins, S. Li, and M. B. Smith, "SAR and B1 field distributions in a heterogeneous human head model within a birdcage coil," *Magnetic Resonance in Medicine*, vol. 40, pp. 847-856, 1998.

[11] Z. Wang and J. C. Lin, "SAR calculations in MRI scanning systems," *IEEE Microwave Magazine*, vol. 13, pp. 22-29, 2012.

[12] H. S. Ho, "Safety of metallic implants in magnetic resonance imaging," *J. Magn. Reson. Imaging*, vol. 14, pp. 472-477, 2001.

[13] J. A. Nyenhuis, S. M. Park, and R. Kamondetdacha, "MRI and implanted medical devices: basic interactions with an emphasis on heating," *IEEE Trans. Dev. Mat. Reliab*., vol. 5, pp. 467-480, 2005.

[14] S. M. Park, R. Kamondetdacha, A. Amjad, and J. A. Nyenhuis, "MRI safety: RF induced heating on straight wires," *IEEE Trans. Magn*., vol. 41, pp. 4197-4199, 2005.

[15] M. A. Stuchly, H. Abrishamkar, and M. L. Strydom, "Numerical evaluation of radio frequency power deposition in human models during MRI," *Proc. IEEE EMBS Int. Conf*., New York City, USA, pp. 272-275, 2006.

[16] S. Pisa, G. Calcagnini, M. Cavagnaro, E. Piuzzi, E. Mattei, and P. Bernardi, "A study of the interaction between implanted pacemakers and the radio frequency field produced by magnetic resonance imaging apparatus," *IEEE Trans. Electromag. Compat*., vol. 50, pp. 35-42, 2008.

[17] S. Pisa, P. Bernardi, M. Cavagnaro, and E. Piuzzi, "Power absorption and temperature elevation produced by magnetic resonance apparatus in the thorax of patients with implanted pacemakers," *IEEE Trans. Electromag. Compat*., vol. 52, pp. 32-40, 2010.

[18] J. T. Vaughan, G. Adriany, M. Garwood, E. Yacoub, T. Duong, L. Dela Barre, P. Andersen, and K. Ugurbil, "Detunable transverse electromagnetic (TEM) volume coil for high-field NMR," *Magnetic Resonance in Medicine*, vol. 47, pp. 990-1000, 2002.

[19] G. Bodganov and R. Ludwing, "Coupled microstrip line transverse electromagnetic resonator model for high-field magnetic resonance imaging," *Magnetic Resonance in Medicine*, vol. 47, pp. 579-593, 2002.

[20] M. Alecci, C. M. Collins, M. B. Smith, and P. Jezzard, "Radio frequency magnetic field mapping of a 3 tesla birdcage coil: experimental and theoretical dependence on sample properties," *Magnetic Resonance in Medicine*, vol. 46, pp. 379-385, 2001.

[21] J. R. Gimbel, "Magnetic resonance imaging of implantable cardiac rhythm devices at 3.0 tesla," *Pacing Clin. Electrophysiol*, vol. 31, pp. 795-801, 2008.

[22] F. G. Shellock, J. Begnaud, and D. M. Inman, "Vagus nerve stimulation therapy system: in vitro evaluation of magnetic resonance imaging-related heating and function at 1.5 and 3 tesla," *Neuromodulation*, vol. 9, pp. 204-213, 2006.

[23] M-A. Golombeck and O. Dossel, "MR-tomography on patients with heart pacemakers – a numerical study," *Proc. IEEE EMBS Int. Conf*., San Francisco, USA, pp. 1076-1079, 2004.

[24] J. C. Lin, P. Bernardi, S. Pisa, M. Cavagnaro, and E. Piuzzi, "Antennas for medical therapy and diagnostics," *in Modern Antenna Handbook*, ed. C. Balanis, Wiley, pp. 1377-1428, 2008.

[25] A. Christ, W. Kainz, E. G. Hahn, K. Honegger, M. Zefferer, E. Neufeld, W. Rascher, R. Janka, W. Bautz, J. Chen, B. Kiefer, P. Schmitt, H-P. Hollenbach, J. Shen, M. Oberle, D. Szczerba, A. Kam, J. W. Guag, and N. Kuster, "The virtual family development of surface-based anatomical models of two adults and two children for dosimetric simulations," *Phys. Med. Biol*., vol. 55, pp. 23-38, 2010.

[26] E. Mattei, M. Triventi, G. Calcagnini, F. Censi, W. Kainz, G. Mendoza, H. I. Bassen, and P. Bartolini, "Complexity of MRI induced heating on metallic leads: experimental measurements of 374 configurations," *Biomedical Engineering OnLine*, 7: 11, 2008.

[27] A. L. Aguilera, Y. V. Volokhina, and K. L. Fisher, "Radiography of cardiac conduction devices: a comprehensive review," *RadioGraphics*, vol. 31, pp. 1669-1682, 2011.

[28] S. Pisa, M. Cavagnaro, E. Piuzzin, and V. Lopresto, "Numerical-experimental validation of a GM-FDTD code for the study of cellular phones," *Microwave Opt. Technol. Lett*., vol. 47, pp. 396-400, 2005.

[29] A. Taflove and S. C. Hagness, *Computational Electrodynamics: The Finite-Difference Time-Domain Method*, Boston, MA: Artech House, 2000.

[30] D. Andreuccetti, R. Fossi, and C. Petrucci, "An internet resource for the calculation of the dielectric properties of body tissues in the frequency range 10 Hz - 100 GHz," *Internet document; URL:http://niremf.ifac.cnr.it/tissprop/*.

[31] H. H. Pennes, "Analysis of tissue and arterial blood temperatures in resting forearm," *J. Appl. Physiol*., vol. 1, pp. 93-122, 1948.

[32] P. Bernardi, M. Cavagnaro, S. Pisa, and E. Piuzzi,

"Specific absorption rate and temperature elevation in a subject exposed in the far-field of radio-frequency sources operating in the 10-900 MHz range," *IEEE Trans. Biomed. Eng*., vol. 50, pp. 295-304, 2003.

[33] S. Pisa, M. Cavagnaro, E. Piuzzi, P. Bernardi, and J. C. Lin, "Power density and temperature distributions produced by interstitial arrays of sleeved-slot antennas for hyperthermic cancer therapy," *IEEE Trans. Microwave Theory Tech*., vol. 51, pp. 2418-2426, 2003.

[34] URL: http://www.itis.ethz.ch/itis-for-health/tissue-properties/database/.

[35] S. Oh, Y-C. Ryu, G. Carluccio, C. T. Sica, and C. M. Collins, "Measurement of SAR-induced temperature increase in a phantom and in vivo with comparison to numerical simulation," *Magnetic Resonance in Medicine*, vol. 71, pp. 1923-1931, 2014.

[36] F. G. Shellock, S. Valencerina, and L. Fischer, "MRI-related heating of pacemaker at 1.5- and 3-tesla: evaluation with and without pulse generator attached to leads," *Circulation*, vol. 112: Supplement II, pp. 561, 2005.

[37] S. Tungjitkusolmun, V. R. Vorperian, N. Bhavaraju, H. Cao, J. Z. Tsai, and J. G. Webster, "Guidelines for predicting lesion size at common endocardial locations during radio-frequency ablation," *IEEE Trans. Biomed. Eng*., vol. 48, pp. 194-201, 2001.

[38] Z. Cao, J. Park, Z-H. Cho, and C. M. Collins, "Numerical evaluation of image homogeneity, signal-to-noise ratio, and specific absorption rate for human brain imaging at 1.5, 3, 7, 10.5, and 14 T in an 8-channel transmit/receive array," *J. Magn. Reson. Imaging*, DOI 10.1002/jmri.24689, pp. 1-7, 2014.

Stefano Pisa received the Electronic Engineering and Ph.D. degrees from the University of Rome "La Sapienza," Rome, Italy, in 1985 and 1988, respectively. In 1989, he joined the Department of Electronic Engineering, University of Rome "La Sapienza," as a Researcher. Since 2001, he has been an Associate Professor with the same university. His research interests are the interaction between electromagnetic fields and biological systems, therapeutic and diagnostic applications of electromagnetic fields, and the modeling and design of MW circuits. He has authored over 150 scientific papers and numerous invited presentations at international workshops and conferences. He serves as a Reviewer for different international journals. He is currently "Consulting Member" of the "Scientific Committee on Physics and Engineering" of the "International Commission on Non-Ionizing Radiation Protection" and a Member of the Advisory Group of the Dutch project "Electromagnetic Fields and Health".

Emanuele Piuzzi received the M.S. (cum laude) and Ph.D. degrees in Electronic Engineering from Sapienza University of Rome, Rome, Italy, in 1997 and 2001, respectively. He is currently an Assistant Professor in Electrical and Electronic Measurements with the Department of Information Engineering, Electronics and Telecommunications (DIET), Sapienza University of Rome. He is the co-author of over 100 publications.

His current research activities include the measurement of complex permittivity of materials, time domain reflectometry applications, biomedical instrumentation design, evaluation of human exposure to electromagnetic fields. Piuzzi is a Member of the Italian Group of Electrical and Electronic Measurements (GMEE) and of the Italian Electrotechnical Committee (CEI). He serves as a Reviewer for several international journals, mainly in the field of instrumentation and measurement.